

Content from this work may be used under the terms of the CC BY 3.0 licence (© 2019). Any distribution of this work must maintain attribution to the author(s), title of the work, publisher, and DOI.

# NEW INSIGHTS IN THE QUENCH MECHANISMS IN NITROGEN DOPED CAVITIES\*

D. Bafia<sup>1†</sup>, A. Grassellino, A. Romanenko, O. S. Melnychuk, D. A. Sergatskov, D. Bice,  
 Fermi National Accelerator Laboratory, Batavia, USA  
 A. D. Palczewski, Jefferson Laboratory, Newport News, USA  
 D. Gonnella, SLAC National Accelerator Laboratory, USA  
 J. F. Zasadzinski, <sup>1</sup>Illinois Institute of Technology, Chicago, USA

## Abstract

This paper will cover a systematic study of the quench in nitrogen doped cavities: three cavities were sequentially treated/reset with different doping recipes which are known to produce different levels of quench field. Analysis of mean free path and TMAP coupled with sample analysis reveals new insights on the physics of the premature quench in nitrogen doped cavities; new recipes demonstrate the possibility to increase quench fields well beyond 30 MV/m.

received a new, optimized 2/0 N-doping treatment proposed by FNAL and were retested. Another 40 μm EP followed and the cavities were tested after receiving a final surface treatment, 3/60 N-doping, as proposed by Jefferson Laboratory. Note that all doping treatments were followed by a 5 μm EP removal to eliminate any nitrides that form on the surface. This leaves nitrogen to exist only as interstitial near the RF surface.

## INTRODUCTION

Nitrogen doping is a surface treatment for niobium superconducting radio-frequency (SRF) cavities capable of producing ultra-high quality factors and very low BCS surface resistance, thereby decreasing the cryogenic load and ultimately driving the cost of machines down [1-3]. However, cavities subject to this surface treatment experience a lower quench field (~27 MV/m) than obtained with other treatments (+40 MV/m) [4, 5]. In addition, N-doped cavities show an increase in sensitivity to trapped magnetic flux when compared to other treatments [6, 7].

In the context of LCLS-II High Energy upgrade and Fermilab R&D, this work presents a sequential study of new, optimized nitrogen doping surface treatments for the minimization of sensitivity to trapped magnetic flux and surface resistance while maximizing quench fields. In addition, TMAP studies were performed and cavity parameters are compared with trends found in [6] to gain insight on the mechanisms responsible for the increased performance that arises from these surface treatments. Lastly, the results of a 9-cell TESLA shaped Nb SRF cavity subject to one of these optimized nitrogen doping treatments is presented.

Table 1: Nitrogen Doping Treatments

2/6 Doping-Baseline	2/0 Doping-FNAL	3/60 Doping-JLab
800 C 3h in UHV	800C 3h in UHV	800 C 3h in UHV
800 C 2min 25 mTorr N	800 C 2min 25 mTorr N	800 C 3min 25 mTorr N
800C 6min UHV	N/A	800C 60min UHV
5 μm EP	5 μm EP	5 μm EP

## RESULTS AND DISCUSSION

### Sequential Study of Single Cells

The performance for one of the three single cell cavities post the sequential treatments outlined in the previous section is summarized in Figure 1.

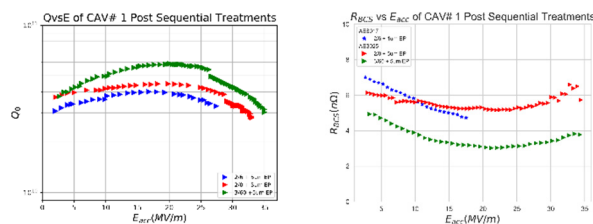


Figure 1: (Left) Quality factor vs accelerating gradient measurements and (Right) BCS resistance vs accelerating gradient of CAV# 1 post sequential treatments. Note cavity # 1 has the serial number AES025.

## CAVITY PREPARATION

Three 1.3 GHz niobium SRF cavities were subject to sequential surface treatments to ensure the same surface morphology. The treatments are outlined in Table 1. First, each of the cavities was baselined with the successfully implemented LCLS-II 2/6 N-doping surface treatment and tested at FNAL's vertical test stand (VTS). Then, the cavities underwent a 40 μm removal of the RF surface via electropolish (EP) to reset it. After this removal, the cavities

Cavity# 1 post the 2/6 doping LCLS II baseline gave a quench field of 27.5 MV/m with a max Q<sub>0</sub> of 4E10. After resetting the cavity surface and treating with 2/0 doping, the quench field increased by about 6 MV/m, giving a final

\* This work was supported by the United States Department of Energy, Offices of High Energy Physics and Basic Energy Sciences under Contracts No. DE-AC05-06OR23177 (Fermilab), No. DE-AC05-06OR23177 (Jefferson Lab), and No. DE-AC02-76F00515 (SLAC).  
 † dbafia@fnal.gov

quench field of 33 MV/m and a max  $Q_0$  of about  $4.4E10$ . Performing another RF surface reset and treating with 3/60 doping gave a quench field of an unprecedented value of 35 MV/m and  $Q_0$  of  $5.9E10$ . Note that the sudden drop in  $Q_0$  at high gradients post 2/0 and 3/60 N-doping occurred after soft quench and is attributed to trapped flux. Processing increased the gradients to their final values. The BCS surface resistance for the cavity post 2/0 nitrogen doping is like that of a standard 2/6 nitrogen doped cavity. However, 3/60 doping gives a very low BCS resistance, achieving a minimum of  $3.5 \text{ n}\Omega$  at 21 MV/m.

The quench field and  $Q_0$  at 16 MV/m for each of the three cavities used in this sequential study are depicted in Figure 2. Doping the three cavities with the baseline 2/6 treatment gives an average quench field of 24 MV/m and average  $Q_0$  at 16 MV/m of  $3.61E10$  for the three cavities studied. Doping with the 2/0 surface treatment increases the average quench field and  $Q_0$  at 16 MV/m up to 27 MV/m and  $4.17E10$ . Lastly, 3/60 N-doping increases these values up to 30 MV/m and  $4.92E10$ .

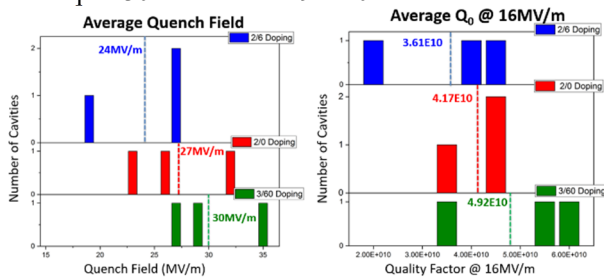


Figure 2: A histogram of (Left) the quench field and (Right) the quality factor at 16 MV/m for each of the three studied cavities post optimized N-doping surface treatments. Dashed lines denote average values.

### TMAP Studies

Using the experimental thermometry mapping (TMAP) setup discussed in [8], the heating profiles of cavity# 1 post sequential optimized N-doping treatments were studied. The 3/60 N-doping plus  $10 \mu\text{m}$  of removal surface via EP treatment was first studied. The resulting  $Q_0$  vs  $E_{\text{acc}}$  curve and TMAP profile taken just before quench are shown in Figure 3.

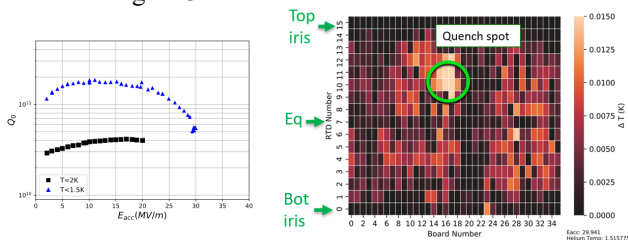


Figure 3: (Left)  $Q_0$  vs  $E_{\text{acc}}$  curve of cavity# 1 post the 3/60+ $10 \mu\text{m}$  EP surface treatment. (Right) TMAP profile taken just before quench with a helium bath temperature of  $\sim 1.5 \text{ K}$ . Note that data was only taken up to 20 MV/m for  $T = 2 \text{ K}$  to avoid quench.

The cavity quenched at 30 MV/m. Inspection of the heating profile just before quench shows that the quench spot was above the equator, but there was uniform heating over the surface. After a  $40 \mu\text{m}$  EP reset of surface, cavity# 1

received 2/0 N-doping plus  $5 \mu\text{m}$  of EP. The RF and TMAP test results are shown in Figure 4. The cavity quenched at 18 MV/m, which is far earlier than was obtained for the first time this cavity received this same surface treatment, as shown in Figure 1 and Figure 2. Further investigation of the furnace RGA scans showed that there were higher levels of impurities because the furnace had not been baked out for several months. As such, this nitrogen doping treatment is labelled as a failed 2/0 N-doping treatment; however, lessons may still be learned from the TMAP profile.

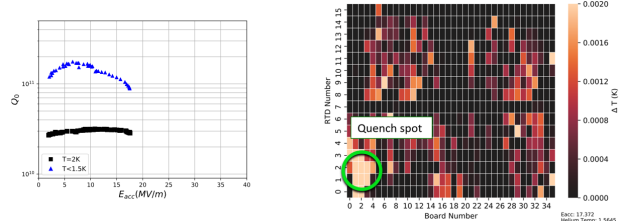


Figure 4: (Left)  $Q_0$  vs  $E_{\text{acc}}$  curve of cavity# 1 post of the failed N-doping treatment of 2/0+ $5 \mu\text{m}$  EP. (Right) TMAP profile taken just before quench with a helium bath temperature of  $\sim 1.5 \text{ K}$ .

The heating profile shown in Figure 4 shows that there was very strong local heating near the bottom iris. The quench spot was located at the point of strongest pre-heating.

The surface of cavity# 1 was reset with another  $40 \mu\text{m}$  EP and was treated to a successful 2/0+ $5 \mu\text{m}$  EP nitrogen doping run. The testing results are displayed in Figure 5. This time, the cavity quenched at the very high accelerating gradient of 38 MV/m at  $T < 1.5 \text{ K}$ . The quench spot of the cavity was just above the cavity equator. It is interesting to see that the point of strongest local pre-heating just before quench does not correspond to the quench spot.

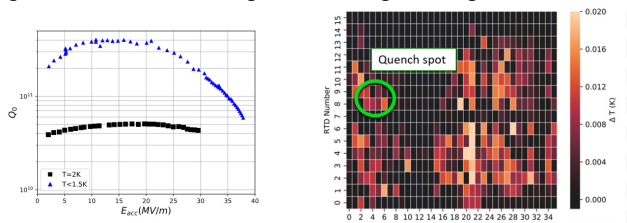


Figure 5: (Left)  $Q_0$  vs  $E_{\text{acc}}$  curve of cavity# 1 post 2/0+ $5 \mu\text{m}$  EP N-doping. (Right) TMAP profile taken just before quench with a helium bath temperature of  $\sim 1.5 \text{ K}$ . Note that data was taken up to 30 MV/m for  $T = 2 \text{ K}$ .

For the final test, cavity# 1 received an additional  $2 \mu\text{m}$  of EP, resulting in a doping treatment of 2/0+ $7 \mu\text{m}$  EP. The results are displayed in Figure 6. The additional  $2 \mu\text{m}$  of EP appears to have drastically lowered the effect of nitrogen doping; the anti-Q slope has been replaced with the high field Q-slope (HFQS). Note, however, that the onset of the HFQS is about 10 MV/m higher than for standard EP cavities, which occurs at  $\sim 25 \text{ MV/m}$ . The TMAP profile taken just before quench shows that the cavity quenched below the equator. It is interesting to see that as the cavity quenches at higher accelerating gradients, the location of quench tends to be closer to the equator.

Content from this work may be used under the terms of the CC BY 3.0 licence (© 2019). Any distribution of this work must maintain attribution to the author(s), title of the work, publisher, and DOI.

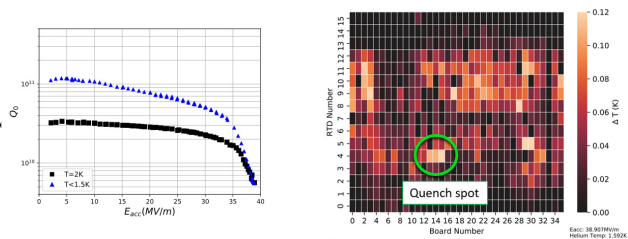


Figure 6: (Left)  $Q_0$  vs  $E_{acc}$  curve of cavity# 1 post 2/0+7  $\mu\text{m}$  EP. (Right) TMAP profile taken just before quench with a helium bath temperature of  $\sim 1.5$  K.

To gain more insight on the mechanisms responsible for the quenches, the heating profiles as a function of the magnetic field of the RTD located closest to the positions of quench for each respective test are shown in Figure 7.

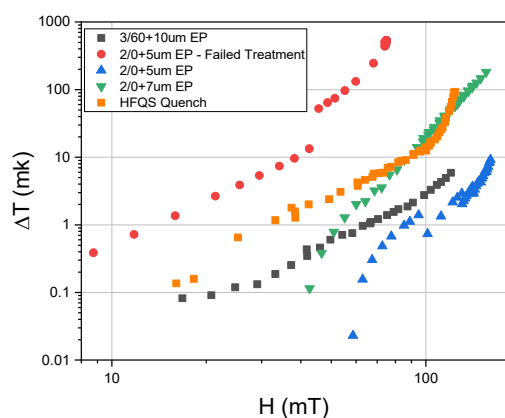


Figure 7: A log vs log plot of the measured temperature difference as a function of the peak magnetic field of the RTD located closest to the position of quench for each of the above TMAP studies. The heating profile of a cavity with high field Q-slope is shown for comparison.

Both the 3/60+10  $\mu\text{m}$  EP and successful 2/0+5  $\mu\text{m}$  EP N-doping treatments show very little pre-heating before quench, with the highest temperature measured below 0.01K. Due to this lack of pre-heating, the quench mechanism of these tests is likely to be of magnetic origin. The quench location of the failed 2/0+5  $\mu\text{m}$  EP N-doping, however, shows much stronger pre-heating, which starts at  $\sim 8$  mT. The heating increases with the peak magnetic field until 40 mT, where there a discrete jump occurs in the heating up to higher values. After this jump, the temperature continues to increase with field, reaching a temperature increase of  $\sim 1$  K. This discrete jump coupled with the strong heating might be indicative of the fact that the quench is due to the heating of a nitride that exists on the surface. The last temperature profile studied is that of the cavity# 1 post 2/0+7  $\mu\text{m}$  EP N-doping. The heating increases quickly with the peak magnetic field, reaching 0.2 K just before quench. As such, the quench might be of thermo-magnetic origins.

The  $Q_0$  vs  $E_{acc}$  curve of this last test post 2/0+7  $\mu\text{m}$  EP N-doping showed the onset of HFQS; as such, it is interesting to compare the heating profile of a cavity with strong HFQS. From Figure 7, it is seen that the heating profile of

cavities subject to HFQS experience a slope that is not as steep as the one observed in the 2/0+7  $\mu\text{m}$  EP N-doping case. However, there is a sharp increase in the slope at 100 mT. This behavior is not observed in the 2/0+7  $\mu\text{m}$  EP surface treatment even though HFQS is present.

### Trends with Mean Free Path

The mean free path (MFP) in a superconductor is set by the distance between impurities and has been found to have some trend with cavity parameters, two of which are the temperature dependent BCS resistance and the sensitivity to trapped magnetic flux. The MFP for some of the above cavities was obtained by measuring the cavity resonant frequency as a function of temperature through warm up. The change in frequency was converted to a change in the penetration depth of the cavity. The resulting data was fit with the SRIMP code [9]. The resulting data is plotted in Figure 8.

An optimal doping treatment should have a mean free path such that it minimizes the sensitivity to trapped magnetic flux and the BCS surface resistance.

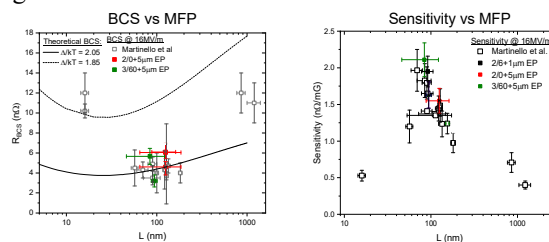


Figure 8: (Left) A plot of BCS surface resistance vs the mean free path near the RF surface of the cavity where supercurrents flow. The solid and dashed lines are the theoretical curves calculated using BCS theory for superconducting gap values of 2.05 and 1.85, respectively. (Right) A plot of sensitivity vs mean free path. Mean free path values of  $>800$  nm come from EP cavities while MFP values  $<20$  nm are those of 120 C bake cavities.

The 2/0 N-doping surface treatment gives a MFP of  $\sim 120$  nm whereas 3/60 N-doping gives MFPs closer to  $\sim 90$  nm. This suggests that although the BCS resistance of cavities subject to 3/60 N-doping is lower than that of 2/0 N-doping, the sensitivity to trapped magnetic flux is higher.

### 2/0 Doping of 1.3 GHz 9-Cell Cavities

The treatment of 1.3 GHz niobium 9-cell SRF cavities to 2/0 N-doping is now discussed. The  $Q_0$  vs  $E_{acc}$  results of the first 9-cell cavity, CAV0017, are shown in blue in Figure 9. The measurements of the cavity showed that although  $Q_0$  was high, reaching a maximum value of  $\sim 3.6E10$ , the cavity quenched at 20 MV/m, lower than the average quench field obtained from the three single cell tests subject to the same surface treatment (27 MV/m). To gain insight on possible causes of early quench, the cavity was equipped with second sound and retested. In addition, mode measurements were performed, allowing for estimates of quench fields in each cell, which are shown in

Table 2. Note that the field distributions in cells symmetric about cell five (cells one & nine, cells two & eight, etc.) are identical. One can see that cell number one, the cell closest to the fundamental power coupler (FPC), was quenching at 20 MV/m. The quench field for each subsequent cell increased until cell number five, which quenched at 32.8MV/m. One possible hypothesis for this difference in quench fields among subsequent cells was that it could stem from variations in surface treatment. Upon investigation of the cavity treatment in the furnace, it was found that cell number one, the early quenching cell, was placed closest to the nitrogen inlet, which sits closest to the door of the furnace.

To investigate this early quench further, the cavity surface was reset with a 60  $\mu\text{m}$  EP and treated once again with the same 2/0 doping treatment as before; however, the cavity orientation was flipped such that the FPC faced the rear of the furnace, i.e., cell number nine was the cell closest to the furnace door/nitrogen inlet. The cavity was retested with second sound and mode measurements. The results are displayed in Figure 9 and Table 2.

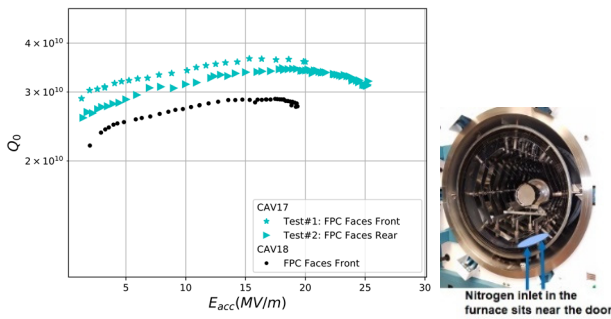


Figure 9: (Left)  $Q_0$  vs  $E_{acc}$  of CAV0017 and CAV0018 taken after 2/0 doping with different orientations in the furnace. (Right) Picture of FNAL furnace. Note that the nitrogen inlet sits close to the furnace door.

Table 2: Estimate of CAV0017 Quench Fields with Cavity Orientation in Furnace

Cell #	Quench Field w/ FPC Toward Front of Furnace [MV/m]	Quench Field w/ FPC Toward Rear of Furnace [MV/m]
1	20	>25.3
2	26.4	>25.3
3	>30	37.2
4	>27	>32.5
5	32.8	36.7
6	>27	>32.5
7	>30	>37
8	>26.4	>25.3
9	>20	25.3

After flipping the orientation of the cavity in the furnace, the quenching cell moved from cell number one to cell number nine. In addition, the quench field increased by about 5 MV/m. This suggests that one possible cause for

early quench could be due to some variation in surface impurity concentration between the two tests between the subsequent cells. The cell closest to the nitrogen inlet could be receiving more nitrogen, causing that particular cell to be overdoped, resulting in an early quench.

To investigate this possibility, a second 9-cell cavity, CAV0018, was also treated to the 2/0+7  $\mu\text{m}$  EP N-doping surface treatment. The cavity was equipped with second sound and mode measurements were performed. The  $Q_0$  vs  $E_{acc}$  curve is shown in Figure 9. An estimate of the quench field for each cell is given in Table 3.

Table 3: Estimate of CAV0018 quench fields. Cell number one was closest to the nitrogen inlet when receiving doping treatment in the furnace.

Cell #	Quench Field (MV/m)
1	19.5
2	30.8
3	>25.3
4	>23.3
5	>30.8
6	>23.3
7	25.3
8	>30.8
9	>19.5s

CAV0018 quenched at 19.5 MV/m and it was found that once again, cell number one, the cell closest to the nitrogen inlet in the furnace while receiving the doping treatment, was the limiting cell. Again, the quench field was found to increase with each subsequent cell toward the center.

To find the quench spot, CAV0018 was equipped with fast thermometry and retested with mode measurements. The measurements showed the quench spot was once again in cell number one and located between sensors 4 and 5, as shown in Figure 10, which is diametrically opposite from the fundamental power coupler.

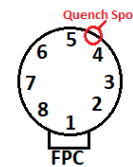


Figure 10: Position of fast thermometry sensors placed on cell number one of CAV0018.

To investigate the origins of quench, samples from each of the cells were cut from the equator to be analyzed using secondary ion mass spectroscopy (SIMS). The location of each cavity cutout is shown in Figure 11. Upon visual inspection, the grains in the cutout from the equator of cell number one, the limiting cell, were much larger than the for the cutout from cell number five, hinting at differences EP removal.

Content from this work may be used under the terms of the CC BY 3.0 licence (© 2019). Any distribution of this work must maintain attribution to the author(s), title of the work, publisher, and DOI.

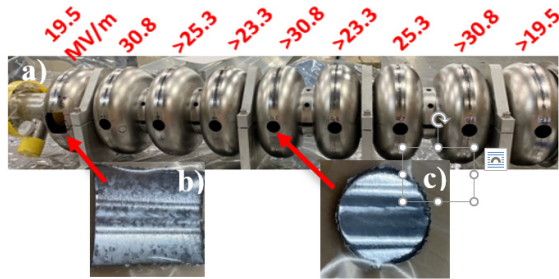


Figure 11: (a) Location of cavity cutouts from the equator of each cell along with the estimated quench field. (b) Cavity cutout from the quench spot in cell one. (c) Cavity cutout from cell number five.

Samples from cell number one (the limiting cell) and cell number five were used in SIMS analysis. The results of the SIMS analysis are shown in Figure 12.

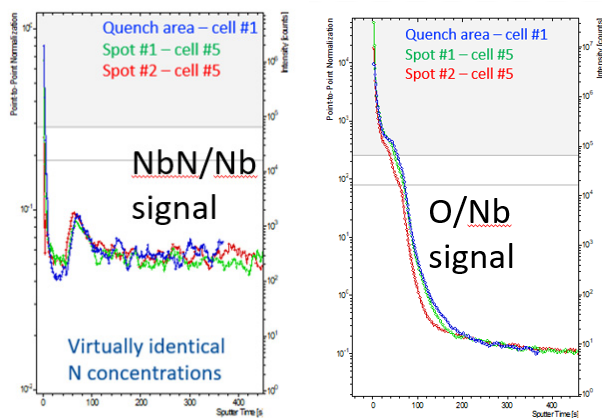


Figure 12: SIMS scans of samples cut from the equators of cells numbers one (quench area, shown in blue) and five (two different areas, shown in green and red). (Left) the NbN signal normalized to the Nb signal. (Right) the oxygen signal normalized to the Nb signal.

SIMS analysis found no difference in the concentration of nitrogen between the studied samples. In fact, the concentration profiles of oxygen, chlorine carbon, sulfur, and fluorine between the two samples was identical. As such, the differences in quench between the subsequent cells cannot be attributed to differences in nitrogen concentration at the equator of the cells of CAV0018. Although there are no differences in nitrogen concentration at the equator between cells one and five, there might be differences closer to the iris. More samples closer to the iris of each cell are currently being cut and will be analyzed using SIMS.

## CONCLUSION

The above discussed optimized nitrogen doping surface treatments of single cell SRF cavities allow for higher accelerating gradients and quality factors than the already exceptional LCLS-II 2/6 N-doping treatment. For single

cells, the new N-doping treatments maintain sensitivity to trapped magnetic flux similar to that of the 2/6 baseline while maintaining or decreasing the BCS resistance. TMAP studies show that the quench mechanism in nitrogen doped cavities is likely to be of magnetic or thermo-magnetic origins. SIMS analysis performed on cutouts from the equators of the first and fifth cells of a nitrogen doped 9-cell cavity shows that there is no difference nitrogen concentration between them. This leaves the cause of early quench in 9-cell cavities still unknown. Successful implementation of optimized nitrogen doping of 9-cell cavities requires further material analysis to understand if there exist differences in surface impurity structures between cells to gain insights on possible quench limitations.

## REFERENCES

- [1] A. Grassellino *et al.*, *Supercond. Sci. Technol.*, **26**, 102001 (2013).
- [2] A. Romanenko, A. Grassellino, A. C. Crawford, D. A. Sergatskov, and O. Melnychuk, *Appl. Phys. Lett.*, **105**, 234103 (2014).
- [3] D. Gonnella *et al.*, “RF Performance of Nitrogen-Doped Production SRF Cavities for LCLS-II”, in *Proc. 8<sup>th</sup> Int. Part Accelerator Conf (IPAC’17)*, Copenhagen Denmark, May 2017, pp. 1156-1159.  
doi: 10.18429/JACoW-IPAC2017-MOPVA128.
- [4] A. Romanenko, A. Grassellino, F. Barkov, and J. P. Ozelis, *Phys. Rev. Spec. Top. Accel. Beams*, **16**, 012001 (2013).
- [5] A. Grassellino *et al.*, *Supercond. Sci. Technol.*, **30**, 094004 (2017).
- [6] M. Martinello *et al.*, *Appl. Phys. Lett.*, **109**, 062601 (2016).
- [7] M. Checchin *et al.*, *Appl. Phys. Lett.*, **112**, 072601 (2018).
- [8] M. Martinello *et al.*, “Magnetic Flux Expulsion in Horizontally Cooled Cavities”, in *Proc. 17<sup>th</sup> Int. Conf. RF Superconductivity (SRF’15)*, Whistler, Canada, Sep. 2015, paper MOPB014, pp. 110-114.
- [9] J. Halbritter, KFK-Extern 3/70–6, 1970.